

Control and Powertrain Management for MultiAutonomous Hybrid Vehicles

Masood Ghasemi

Department of Engineering Technology and Industrial Distribution, Texas A&M University, College Station, TX 77843 e-mail: MGhasemi.Academic@gmail.com

Xingyong Song

Department of Engineering Technology and Industrial Distribution;
Department of Mechanical Engineering,
Texas A&M University,
College Station, TX 77843
e-mail: songxy@tamu.edu

The need for less fuel consumption and the trend of higher level of autonomy together urge the power optimization in multihybrid autonomous vehicles. Both the multivehicle coordination control and the hybrid powertrain energy management should be optimized to maximize fuel savings. In this paper, we intend to have a computationally efficient framework to optimize them individually and then evaluate the overall control performance. The optimization is conducted in series. First is at the multivehicle system's level where the distributed locally optimal solution is given for vehicles with nonlinear dynamics. Second, the powertrain management optimization is conducted at the hybrid powertrain level. We provide an analytical formulation of the powertrain optimization for each hybrid vehicle by using Pontryagin's minimum principle (PMP). By approximating the optimal instantaneous fuel consumption rate as a polynomial of the engine speed, we can formulate the optimization problem into a set of algebraic equations, which enables the computationally efficient real-time implementation. To justify the applicability of the methodology in real-time, we give directions on numerical iterative solutions for these algebraic equations. The analysis on the stability of the method is shown through statistical analysis. Finally, further simulations are given to confirm the efficacy and the robustness of the proposed optimal approach. An off-road example is given in the simulation, although the framework developed can be applied to on-road scenario as well.

[DOI: 10.1115/1.4043110]

1 Introduction

The need for lower fuel consumption and cleaner powertrain operation has increased the demand for hybrid vehicles. Meanwhile, the emerging trend of connected and autonomous vehicles requests more cooperative operation among the vehicles. This is a trend not only for on-road passenger transportation but also for off-road vehicles like naval, aerospace, military, and commercial application. Thus, being able to effectively minimizing fuel consumption in a cooperative environment is a critical task to achieve.

For an autonomous hybrid vehicle under cooperative control, there are typically two layers of energy optimization. The first is the vehicle level coordination, where the vehicle trajectory is optimized based on a cooperative control strategy. The second is the powertrain energy management (power split) optimization among different powertrain components, where the power demand from the driveline is optimally split to the power sources such as engine and motors [1-3]. Considering both these layers together in the control design can bring benefit. It is well known that the optimal energy management of hybrid powertrain can be achieved only if the future vehicle trajectory is known [3]. This requirement is typically nonfeasible for a conventional driver based vehicle, since the intention of the driver cannot be acquired by powertrain control in advance. But the knowledge of future vehicle trajectory can become available for autonomous driving under cooperative control scenario, since the future trajectories and vehicle speeds can be estimated and simulated once the cooperative control strategy/ control law is determined, based on the real-time traffic information.

A hybrid system is usually powered by multiple power sources, a primary and less efficient one (engine) and the auxiliary and more efficient power sources (motor and generator). The existing hybrid architectures [3] include series hybrid, parallel hybrid, and power split hybrid. In this paper, we focus on the widely used power split hybrid, which combines the benefits of series and parallel structures in fuel efficiency optimization [3]. Given the power demand from the vehicle, the engine is controlled to operate close to its optimal region, and the deficit or surplus of the engine power supply is compensated for or stored in the battery. A critical issue to address is how to split the power demand among the power sources (engine and two motors) in real-time, referred to as power split management or powertrain energy management [3]. This is a very challenging control problem, as an improper split may result in significant energy loss, inadequate power supply, or battery drain. Furthermore, minimizing instantaneous energy consumption is not equivalent to optimizing the overall fuel efficiency for the entire driving cycle. Oftentimes, the instantaneous fuel efficiency may need to be sacrificed in order to minimize the overall fuel consumption [3]. Therefore, the powertrain management of a power split hybrid vehicle is a complicated problem requiring knowledge of the future vehicle speed profile to achieve the optimized performance [4]. Optimal energy management strategies such as dynamic programming [4], stochastic dynamic programming [4], equivalent consumption algorithm (ECMS) [3], Pontryagin's minimum principle (PMP) based control [5–10], and model predictive control have been studied, where most of the existing research considers a driver-based single vehicle scenario. The main challenge for the existing energy management approaches is that it is hard to have both computational efficiency and effective optimization to be met at the same time. This challenge becomes more evident for autonomous vehicles under cooperative control, since the vehicle on-board processer needs to handle computational load from both vehicle coordination and powertrain control. Thus, a real-time powertrain management approach that can ensure optimality by effectively leveraging the future driveline torque and speed information provided by the cooperative controller is needed for the power optimization in cooperative hybrid vehicles.

Meanwhile, a multiagent system defines a set of interconnected autonomous subsystems known as agents whose behavior is

¹Corresponding author.

Contributed by the Dynamic Systems Division of ASME for publication in the JOURNAL OF DYNAMIC SYSTEMS, MEASUREMENT, AND CONTROL. Manuscript received March 30, 2018; final manuscript received January 15, 2019; published online May 8, 2019. Assoc. Editor: Junmin Wang.

associated with a specific consensus among themselves [11-14]. The interconnection structure defines the communication topology of the multiagent system, which can be centralized, where the global information is available for all agents, or decentralized or distributed, where only the local information is available for each agent. In this paper, we specifically consider the decentralized case. To optimize the coordination among the agents, the optimal cooperative control was studied extensively. The authors in Ref. [14] developed an inverse optimal solution for a general linear system by introducing the notion of partial stability. The result was extended in Ref. [13], which provided more in-depth formulation on solving the cooperative regulator and multiagent systems tracking. However, their design is only limited to the open loop free response of the agents and cannot be used for the case when the leader agent has an arbitrary trajectory. In Ref. [15], the authors considered a constrained cooperative regulator problem and presented a distributed projected subgradient algorithm so as to give a locally optimal solution. In Ref. [16], the authors used a generalized fuzzy hyperbolic model approximation of the Hamilton-Jacobi equations to obtain the optimal coordination control. However, most existing research on the optimal multiagent control is based on a generic multiagent formulation, considering linear systems such as single or double integrator models and cannot be directly used for general nonlinear systems including the vehicle dynamics model.

The objective of this paper is to provide a computationally efficient framework that considers both the vehicles coordination and their powertrain control. Accordingly, the contributions of the paper are as follows: First, instead of assuming a linear system of single or double integrators like most existing studies on the optimal multi-agent control, the optimization in the multiagent cooperative control is achieved for agents with nonlinear vehicular dynamics based on locally distributed information. The control is first given in a general form for a system consisting of agents with affine Euler-Lagrange dynamics, using feedback linearization. Then, we extend the design to systems with nonlinear vehicular dynamics, by converting the dynamics model into the Euler-Lagrange form through coordinate transformation. Second, the powertrain level optimization is formulated analytically for each hybrid vehicle agent by using the PMP. Different from the previous PMP-based approaches such as Refs. [6] and [8], the optimal control is eventually converted into a set of algebraic equations, instead of differential equations. This is enabled by approximating the optimal instantaneous fuel consumption rate as a polynomial of the engine speed, and it is more promising to be solved and implemented in real-time in a computationally efficient fashion. A fast converging numerical approach for solving the resultant algebraic equations is proposed to justify the fact that the approach can be implemented in real-time. Third, we formulate the vehicles cooperative control and hybrid vehicles powertrain management in the same framework by considering a multiagent system of hybrid vehicle agents. The vehicle future trajectory and driveline torque profile are predicted based on an optimal multiagent cooperative controller, and then the future driveline power demand is fed to the powertrain level controller for energy management.

We use the following notations in this paper. We denote \mathbb{R} as the set of real numbers, \mathbb{R}_+ as the set of positive real numbers, \mathbb{R}_+ as the set of non-negative real numbers, and \mathbb{R}^n as the set of $n \times 1$ column vectors. Furthermore, I_n denote an $n \times n$ identity matrix, $(\cdot)^T$ denote matrix transpose, and $(\cdot)^{-1}$ denote matrix inverse.

The rest of the paper is organized as follows: In Sec. 2, we give the dynamics of a vehicle system. In Sec. 3, we present the formulation of the optimal coordination in a multiagent system. The derivation is given in terms of a general multiagent system and then is extended to the specific case of a multivehicle system with nonlinear vehicular dynamics. In Sec. 4, a hybrid system mechanism is introduced and then a fully analytical derivation of the optimization problem is given using the necessary condition of the PMP.

We give the description on a numerical approach for solving the PMP-based formulation in Sec. 5. Furthermore, we provide simulation examples in Sec. 6. Finally, in Sec. 7, we conclude the discussion by highlighting the contributions of this research work.

2 Model of an Autonomous Vehicle

Consider a typical rear wheel-driven vehicle. In order to avoid dynamical complexity, the reaction forces on each individual wheel are summed up at their midaxles. Equivalently, the free-body diagram of the vehicle is obtained as depicted in Fig. 1. Moreover, to enable an efficient cooperative control design, some of the complex steering mechanism dynamics and wheel slipping dynamics are neglected in the vehicle dynamics model. The detailed derivation of the model is given in the Appendix.

The horizontal and vertical position of the mass center C of the vehicle in the inertial reference frame and its orientation are determined by the variables X, Y, and θ , respectively. The kinematics of the vehicle are given by

$$\dot{X}(t) = v_x(t)\cos\theta(t) - d_r\omega(t)\sin\theta(t), \quad t \ge 0$$
 (1)

$$\dot{Y}(t) = v_x(t)\sin\theta(t) + d_r\omega(t)\cos\theta(t) \tag{2}$$

$$\dot{\theta}(t) = \omega(t) \tag{3}$$

where v_x is the longitudinal velocity, ω is the yaw angular velocity of the vehicle, and $d_r \in \mathbb{R}_+$ is the distance between C and the rear axle. Moreover, the dynamics of the vehicle is given by

$$M(\eta)\dot{\eta}(t) = F(\eta) + G(\eta)T(t), \quad t \ge 0$$
(4)

where $\eta \triangleq [v_x, \omega]^T$ is the velocity vector, and $T \triangleq [T_d, T_s]^T$ is the vector of driving and steering torques

$$M(\eta) \triangleq \begin{bmatrix} \tilde{m} & \frac{I_{\rm f}(d_{\rm f} + d_{\rm r})^2 \omega(t)}{r^2 v_x(t)} \\ 0 & \tilde{I} \end{bmatrix}$$
 (5)

$$F(\eta) \triangleq \begin{bmatrix} md_{\mathsf{r}}\omega^{2}(t) - \frac{1}{2}\rho C_{\mathsf{d}}A_{\mathsf{f}}v_{x}^{2}(t) - f_{\mathsf{t}}mg \\ -md_{\mathsf{r}}\omega(t)v_{x}(t) \end{bmatrix}$$
 (6)

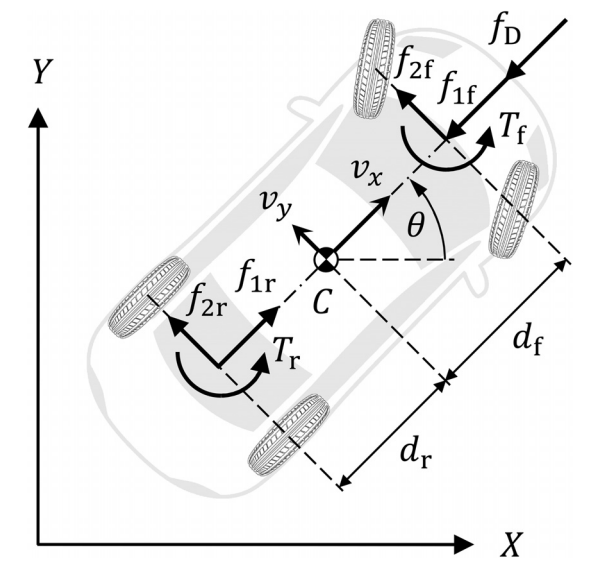


Fig. 1 The free body diagram of a vehicle

$$G(\eta) \triangleq \begin{bmatrix} \frac{1}{r} & -\frac{(d_{\rm f} + d_{\rm r})\omega(t)}{d_{\rm f}v_x(t)} \\ 0 & \frac{d_{\rm f} + d_{\rm r}}{d_{\rm f}} \end{bmatrix}$$
(7)

m is the total mass of the vehicle, I is the yaw moment of inertia of the vehicle, $\tilde{m} \triangleq m + ((I_{\rm f} + I_{\rm r})/r^2)$, $\tilde{I} \triangleq I + m d_{\rm r}^2$, $d_{\rm f} \in \mathbb{R}_+$ is the distance between C and the front axle, $I_{\rm f}$ is the equivalent moment of inertia of the front wheels and the front axle about the axis of the front axle for zero steering angle, $I_{\rm r}$ is the equivalent moment of inertia of the rear wheels and the rear axle plus all internal rotatory components translated at the rear axle about the axis of the rear axle, r is the radius of each wheel, ρ is the density of air, $C_{\rm d}$ is the drag coefficient, $A_{\rm f}$ is the effective frontal area of the vehicle, and $f_{\rm t}$ is the friction coefficient.

3 Optimal Coordination in a Multiagent System

This section presents the concept of control and optimization in multiagent systems with an emphasis on leader following cooperation. First, we advise the design for an Euler–Lagrangian multiagent with affine dynamics structure. The design is based on the availability of the distributed information among agents and it provides the local optimal solution for each agent. Next, we extend the results to a multiagent system of ground vehicles with the nonlinear dynamics presented in Sec. 2, by transforming the specific vehicular dynamics to the Euler–Lagrangian form through coordinate transformation.

3.1 Systems With Affine Euler–Lagrange Dynamics. Consider a multiagent system consisting of a leader agent denoted by 'L' and a set of $p \ge 1$ agents numbered from 1 to p whose individual agent's dynamics are given by

$$M_{i}(q_{i}, \dot{q}_{i})\ddot{q}_{i}(t) = F_{i}(q_{i}, \dot{q}_{i}) + u_{i}(t),$$

$$q_{i}(0) = q_{i0}, \quad \dot{q}_{i}(0) = \dot{q}_{i0}, \quad t \ge 0, \ i = L, 1, ..., p$$
(8)

where $q_i \in \mathbb{R}^n$ is the vector of generalized coordinates of the ith agent; $M_i(q_i,\dot{q}_i) \in \mathbb{R}^{n \times n}$ is the positive definite inertia matrix of the ith agent; $u_i \in \mathbb{R}^n$, $t \geq 0$, is the control input for the ith agent; and $F_i(q_i,\dot{q}_i) \in \mathbb{R}^n$ is the vector of Coriolis, centrifugal, conservative, and nonconservative forces acting on the ith agent. The ensemble of all agents and the leader agent forms a connected digraph [17] by communicating their positions and velocities. More specifically, the digraph contains a spanning tree with the leader agent as its root ensuring that the information originated at the leader distributes to all agents. Accordingly, the sets of the neighboring agents are identified as

$$\mathcal{N}_i \subseteq \{L, 1, ..., p\} \setminus \{i\}, \quad i = 1, ..., p \tag{9}$$

where \mathcal{N}_i represents a set of agents whose positions and velocities are available for the *i*th agent. Furthermore, the distributed error of an agent is defined as the algebraic average of the errors associated with the agent with respect to its neighboring agents. Specifically, we express the distributed errors as

$$z_i(t) \triangleq q_i(t) - \frac{1}{|\mathcal{N}_i|} \sum_{j \in \mathcal{N}_i} (q_j(t) + l_{ij}(t)), \quad i = 1, ..., p$$
 (10)

where $z_i \in \mathbb{R}^n$ is the distributed error of the *i*th agent, $|\mathcal{N}_i| \geq 1$ is the cardinality of \mathcal{N}_i , which is the number of elements in \mathcal{N}_i , and $l_{ij} \in \mathbb{R}^n, i, j \in \{L, 1, ..., p\}$, specify the desired geometry of ensemble of all agents and the leader. The leader following coordination problem can be formulated by rewriting Eq. (8) in terms of the distributed errors. The second time derivative of Eq. (10) yields

$$\begin{split} \ddot{z}_{i}(t) &= M_{i}^{-1}(q_{i}, \dot{q}_{i})u_{i}(t) + M_{i}^{-1}(q_{i}, \dot{q}_{i})F_{i}(q_{i}, \dot{q}_{i}) \\ &- \frac{1}{|\mathcal{N}_{i}|} \sum_{j \in \mathcal{N}_{i}} \left(\ddot{q}_{j}(t) + \ddot{l}_{ij}(t) \right), \\ z_{i}(0) &= z_{i0}, \quad \dot{z}_{i}(0) = \dot{z}_{i0}, \quad t \geq 0, \ i = 1, ..., p \end{split}$$

$$(11)$$

The knowledge of the neighboring agents' acceleration appearing in the right-hand side of Eq. (11) is a necessity in order to achieve the exact coordination among all agents with respect to the leader agent. We assume that such information is available for each agent through robust observer estimation [18,19].

Next, consider a feedback linearization control given as

$$u_{i}(t) \triangleq M_{i}(q_{i}, \dot{q}_{i}) \left(v_{i}(t) + \frac{1}{|\mathcal{N}_{i}|} \sum_{j \in \mathcal{N}_{i}} \left(\ddot{q}_{j}(t) + \ddot{l}_{ij}(t) \right) \right)$$

$$-F_{i}(q_{i}, \dot{q}_{i}), \quad i = 1, \dots, p$$

$$(12)$$

where $v_i \in \mathbb{R}^n$ is the new control input. Substituting Eq. (12) in Eq. (11) gives

$$\ddot{z}_i(t) = v_i(t), \quad z_i(0) = z_{i0}, \quad \dot{z}_i(0) = \dot{z}_{i0}, \quad t \ge 0, \quad i = 1, ..., p$$
(13)

Let $\tilde{z}_i \triangleq [z_i^{\mathrm{T}}(t), \dot{z}_i^{\mathrm{T}}(t)], i = 1, ..., p$. Then, Eq. (13) is rewritten as

$$\dot{\tilde{z}}_i(t) = A + Bv_i(t), \quad \tilde{z}_i(0) = \tilde{z}_{i0} \quad t \ge 0, \quad i = 1, ..., p$$
 (14)

where

$$A \triangleq \begin{bmatrix} 0 & I_n \\ 0 & 0 \end{bmatrix}, \quad B \triangleq \begin{bmatrix} 0 \\ I_n \end{bmatrix}$$
 (15)

We define the distributed control protocol as

$$v_i(t) = -K_i \tilde{z}_i(t), \quad t \ge 0, \quad i = 1, .., p$$
 (16)

where $K_i \in \mathbb{R}^{n \times 2n}$ is the control gain for the *i*th agent. We consider the cost function of the *i*th agent defined as

$$J_i \triangleq \int_0^\infty (\tilde{z}_i^{\mathsf{T}}(t)R_{1i}\tilde{z}_i(t) + v_i^{\mathsf{T}}(t)R_{2i}v_i(t))dt \tag{17}$$

where $R_{1i} \in \mathbb{R}^{2n \times 2n}$ is positive semi-definite, and $R_{2i} \in \mathbb{R}^{n \times n}$ is positive definite. The collision free optimal problem of minimization of J_i , i = 1, ..., p, subject to Eqs. (14)–(16) can be solved by using the linear quadratic regulator (LQR) approach. Specifically, we obtain

$$K_i = B^{\mathrm{T}} P_i, \quad i = 1, .., p$$
 (18)

where $P_i \in \mathbb{R}^{2n \times 2n}$ is the solution of the algebraic Riccati equations given by

$$A^{\mathrm{T}}P_{i} + P_{i}A + R_{1i} - P_{i}BR_{2i}^{-1}B^{\mathrm{T}}P_{i} = 0, \quad i = 1, ..., p$$
 (19)

Note that the above cooperative control design provides only local optimal solution for each agent.

3.2 Systems With Nonlinear Vehicular Dynamics. In this subsection, we will transform the nonlinear vehicular dynamics (1)–(3) and (4) into the affine Euler–Lagrange form, so we can directly use the optimal controller described in the previous subsection for cooperative control design.

Consider the multiagent system consisting of a leader vehicle agent denoted by L and a set of $p \ge 1$ autonomous vehicle agents numbered from 1 to p whose kinematics and dynamics are identical and are given by Eqs. (1)–(3) and (4), respectively. We use index $i \in \{L, 1, ..., p\}$ to indicate the specific dynamics of the

*i*th vehicle agent. In order to adopt the optimal coordination control design discussed earlier, we write the dynamics in terms of the generalized position coordinates, $q_i(t) \triangleq [X_i(t), Y_i(t)]^T$, i = L, 1, ..., p, and the generalized orientation coordinate, $\theta_i(t)$. The time derivative of Eqs. (1) and (2) yields

$$\ddot{q}_{i}(t) = R_{i}(\theta_{i})Q\dot{\eta}_{i}(t) + R_{i}\left(\theta_{i} + \frac{\pi}{2}\right)Q\eta_{i}(t)\omega_{i}(t)$$

$$q_{i}(0) = q_{i0}, \quad \dot{q}_{i}(0) = \dot{q}_{i0}, \quad t \ge 0, \quad i = L, 1, ..., p$$
(20)

where

$$R_{i}(\theta_{i}) \triangleq \begin{bmatrix} \cos \theta_{i}(t) & -\sin \theta_{i}(t) \\ \sin \theta_{i}(t) & \cos \theta_{i}(t) \end{bmatrix}, \quad Q \triangleq \begin{bmatrix} 1 & 0 \\ 0 & d_{r} \end{bmatrix}$$
(21)

Note that the planar rotation matrix, $R_i(\cdot) : \mathbb{R} \to \mathbb{R}^{2\times 2}$, is an orthogonal matrix satisfying the following properties:

$$|R_i(\theta_i)| = 1, \quad \theta_i \in \mathbb{R}$$

$$R_i^{-1}(\theta_i) = R_i^{\mathrm{T}}(\theta_i) = R_i(-\theta_i)$$

$$R_i(\theta_{i1} + \theta_{i2}) = R_i(\theta_{i1})R_i(\theta_{i2}) = R_i(\theta_{i2})R_i(\theta_{i1})$$
(22)

Accordingly, one can write $\eta_i(t) = Q^{-1}R_i^{\mathrm{T}}(\theta_i)\dot{q}_i(t)$. Furthermore, substituting $\dot{\eta}_i(t)$ from Eq. (4) in Eq. (20) gives

$$\ddot{q}_{i}(t) = R_{i}(\theta_{i})QM^{-1}(\dot{q}_{i})\left(F_{i}(\dot{q}_{i}) + G_{i}(\dot{q}_{i})T_{i}(t)\right) + R_{i}\left(\frac{\pi}{2}\right)\dot{q}_{i}(t)\dot{\theta}_{i}(t),$$

$$q_{i}(0) = q_{i0}, \quad \dot{q}_{i}(0) = \dot{q}_{i0}, \quad t \geq 0, \quad i = L, 1, ..., p$$
(23)

where $\dot{\theta}_i(t)$ is obtained from the kinematics of the vehicle agent given by

$$\dot{\theta}_i(t) = \frac{1}{d_r} \left(-\sin \theta_i(t) \dot{X}_i(t) + \cos \theta_i(t) \dot{Y}_i(t) \right)$$

$$\theta_i(0) = \theta_{i0}, \quad i = L, 1, ..., p$$
(24)

In Ref. [20], it is shown that the orientation kinematics given by Eq. (24) is minimum phase with respect to its velocity states, $\dot{X}_i(t)$ and $\dot{Y}_i(t)$. Therefore, the control design for the underactuated vehicle agent can be adopted based on its dynamics given by Eq. (23). One can rewrite Eq. (23) as

$$\tilde{M}_{i}(\dot{q}_{i},\theta_{i})\ddot{q}_{i}(t) = \tilde{F}_{i}(\dot{q}_{i},\theta_{i}) + u_{i}(t)$$

$$q_{i}(0) = q_{i0}, \quad \dot{q}_{i}(0) = \dot{q}_{i0}, \quad t \ge 0, \quad i = L, 1, ..., p$$
(25)

where

$$u_i(t) \triangleq G_i^{-1}(\dot{q}_i)T_i(t) \tag{26}$$

$$\tilde{M}_i(\dot{q}_i, \theta_i) \triangleq M_i(\dot{q}_i) Q^{-1} R_i^{\mathrm{T}}(\theta_i)$$
(27)

$$\tilde{F}_i(\dot{q}_i, \theta_i) \triangleq M_i(\dot{q}_i) Q^{-1} R_i^{\mathrm{T}} \left(\theta_i - \frac{\pi}{2} \right) \dot{q}_i(t) \dot{\theta}_i(t) + F_i(\dot{q}_i)$$
 (28)

Vehicle dynamics given by Eq. (25) conforms to the system representation of Eq. (8). Accordingly, the optimal coordination control design can be developed for the vehicular multiagent system by following the steps described in Sec. 3.1 and the control inputs consisting of the steering torques and the driving rear axle torques are obtained for each vehicle. The steering torques, $T_{si}(t)$, $t \ge 0$, i = 1, ..., p, act as reference inputs for the steering mechanisms of the vehicles. Nonetheless, their utilization requires

the detailed knowledge of steering mechanisms themselves, which is out of the scope of this research work. The driving rear axle torques, $T_{di}(t), t \geq 0, i = 1, ..., p$, provide the torques on demand (at the driveline) for the internal powertrain dynamics of the vehicles. Note that in order to comply with the internal hybrid systems' constraints (described in Sec. 4), and to consider realistic road conditions, the LQR control protocols are constrained limiting the vehicles' accelerations and velocities. Note that since each vehicle's model given by Eqs. (1)–(7) as well as the estimated neighboring vehicles' accelerations bears uncertainties, further analysis on the robustness of the controller is necessary.

Once the optimal cooperative controller is determined, the future vehicle trajectory and driving torques on demand can be estimated and predicted. The prediction for a single vehicle scenario based on the real-time traffic information has been extensively studied in the literature [9], and it is a straightforward extension for the multivehicle case once the cooperative controller is available. Thus, it is not covered in detail here. The current and future driveline torque demands, $T_{di}(t), t \ge 0, i = 1, ..., p$, can be regarded as reference inputs for the internal power optimization of the vehicles, which is the subject of Sec. 4.

4 Powertrain Energy Management in Power Split Hybrid Electric Vehicles

In this section, we will present a real-time computationally efficient approach for the hybrid powertrain management of each vehicle agent. Different from the previous PMP-based approaches for hybrid vehicle, we can formulate the optimal control into a set of algebraic equations rather than differential equations, enabled by approximating the optimal instantaneous fuel consumption rate as a polynomial of the engine speed. This can lead to a real-time numerical solution online.

Let each vehicle agent discussed in Sec. 3.2 be powered by a hybrid system consisting of an internal combustion engine and an electrical battery. A typical mechanism of the power split was introduced by Toyota for Prius vehicles [21]. The schematic of such a system is depicted in Fig. 2. This system also consists of a planetary gear set, a coupler gear set, an inverter, and two electrical machines. The electrical machines can act as either motors or generators allowing two degrees-of-freedom in the system, and thus, setting the engine operation at any arbitrary speed and torque. Assuming that the inertia of the moving components of the hybrid system are negligible, the algebraic equations describing the constraints between these components can be derived by considering the power balances at the planetary gear set, the coupler gear set, and the inverter. For simplicity, we drop the index i associated with each vehicle in the following derivations. Specifically, the power balance at the coupler gear set gives

$$T_{\rm m}(t) = -\left(\frac{r_{\rm r}}{r_{\rm s} + r_{\rm r}}\right) T_{\rm e}(t) + \frac{1}{k_{\rm c}} T_{\rm d}(t)$$
 (29)

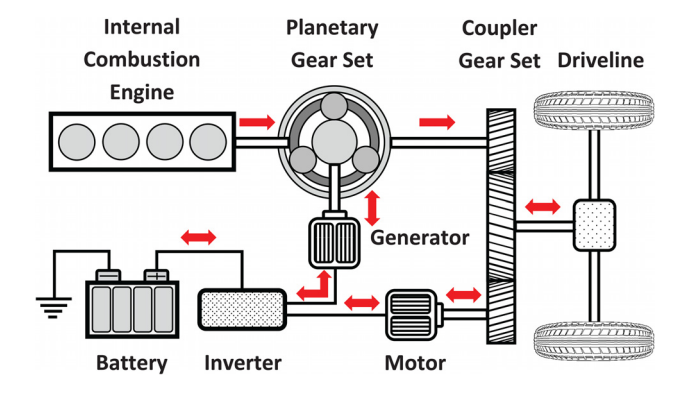


Fig. 2 The hybrid system of power split in Toyota Prius. The arrows indicate power flow directions.

$$\omega_{\rm m}(t) = k_{\rm c}\omega_{\rm d}(t) \tag{30}$$

where $T_e \in \overline{\mathbb{R}}_+$ is the engine's torques, $T_m \in \mathbb{R}$ is the motor's torques, $\omega_m, \omega_d \in \mathbb{R}$ are the motor's and the driveline's speeds, respectively, $r_s, r_r \in \mathbb{R}_+$ are the radii of the sun gear and the ring gear, respectively, and $k_c \in \mathbb{R}_+$ is the gear ratio at the coupler gear set. Similarly, the power balance at the planetary gear set gives

$$T_{\rm g}(t) = -\left(\frac{r_{\rm s}}{r_{\rm s} + r_{\rm r}}\right) T_{\rm e}(t) \tag{31}$$

$$\omega_{\rm e}(t) = \left(\frac{r_{\rm r}}{r_{\rm s} + r_{\rm r}}\right) \omega_{\rm m}(t) + \left(\frac{r_{\rm s}}{r_{\rm s} + r_{\rm r}}\right) \omega_{\rm g}(t) \tag{32}$$

where $T_{\rm g}\in\mathbb{R}$ is the generator's torque and $\omega_{\rm g}\in\mathbb{R}$ is the generator's speeds. Finally, the power balance at the inverter yields

$$P_{b}(t) = \mu_{m}^{k_{m}} T_{m}(t) \omega_{m}(t) + \mu_{g}^{k_{g}} T_{g}(t) \omega_{g}(t)$$
(33)

where $P_b \in \mathbb{R}$ is the battery power, μ_m , $\mu_g \in (0, 1)$ are, respectively, the efficiency factors of the motor and the generator when they are operating as generators, and k_m and/or k_g are equal to "1" if their respective electrical machines are operating as generators, otherwise, they are equal to "-1". Substituting the relations for the motor and the generator's torques and speeds from Eqs. (29) to (32) in Eq. (33) gives

$$P_{b}(t) = \mu_{m}^{k_{m}} T_{d}(t) \omega_{d}(t) - \mu_{g}^{k_{g}} T_{e}(t) \omega_{e}(t) - \frac{k_{c} r_{r} \left(\mu_{m}^{k_{m}} - \mu_{g}^{k_{g}}\right)}{r_{c} + r_{r}} T_{e}(t) \omega_{d}(t)$$
(34)

Furthermore, the dynamics of the battery is given by

$$\dot{s}(t) = -\frac{V_b - \sqrt{V_b^2 - 4R_b P_b(t)}}{2R_b Q_b}, \quad s(0) = s_0, \quad t \ge 0$$
 (35)

where $s \in \mathbb{R}_+$ is the state of the charge of the battery, $V_b \in \mathbb{R}_+$ is the battery's open circuit voltage, $R_b \in \mathbb{R}_+$ is the internal resistance of the battery, and $Q_b \in \mathbb{R}_+$ is the capacity of the battery. Note that for the nominal operating range of the state of the charge of the battery (40–80%), these variables are almost constant [6].

Note that the powertrain variables are all subject to boundary conditions due to physical limitations. In the following derivations, such limitations are implicitly considered. Furthermore, in charge sustaining operations, the utilization of the hybrid system increases the total power that the engine should provide to the driveline. This is first due to the power dissipation through the electrical machines in Eq. (33) and second due to the nonlinear behavior of the battery described by Eq. (35). Nonetheless, such a system can help the engine to operate more efficiently during the entire operation of the vehicle. Therefore, a proper design is required in order to achieve a better overall fuel economy.

We formulate the problem as a nonlinear optimization of the hybrid system by using Pontryagin's minimum principle. The formulation is given for one driving cycle and is repeated for other driving cycles such that it gives overall optimal solution for the entire operation of the vehicle. The formulation assumes that the power demand for the entire driving cycle is known. We suppose that an appropriate prediction scheme provides such information. Since the hybrid system has two degrees-of-freedom, then any two independent variables can be used as the optimization inputs. Let $u(t) \triangleq \left[T_{\rm e}(t), \omega_{\rm e}(t)\right]^{\rm T}, t \geq 0$, denote the vector of optimization inputs. Furthermore, we consider a charge sustaining operation where the initial and final values of the state of the charge of the

battery are equal, and accordingly, the optimization problem is defined as the minimization of the total fuel consumption subject to the dynamical equations of Eq. (35) and the constraints on the powertrain variables. The cost function is written as

$$J \triangleq \gamma(s_{\rm ff} - s(t_{\rm f})) + \int_{t_{\rm f}}^{t_{\rm f}} \dot{m}_{\rm f}(u(t))dt \tag{36}$$

where $J \in \mathbb{R}_+$ is the total cost for the driving cycle initiating at $t_i \in \mathbb{R}_+$ and finalizing at $t_f \in \mathbb{R}_+$, $\dot{m}_f(\cdot) : \mathbb{R}_+^2 \to \mathbb{R}_+$ is a nonlinear function, which gives the instantaneous fuel consumption rate, $s_{rf} = s_0$ is the final value of the state of the charge of the battery, and $\gamma \in \mathbb{R}$ is a constant coefficient, which drives the terminal condition to zero. We write the Hamiltonian as

$$H(t, s, u) \triangleq \dot{m}_{\rm f}(u(t)) - \lambda(t)\dot{s}(t) \tag{37}$$

where $\lambda \in \mathbb{R}$ is the costate. The adjoint equation is derived as

$$\dot{\lambda}(t) = \frac{\partial}{\partial s} H(t, s, u) = 0 \tag{38}$$

$$\lambda(t_{\rm f}) = -\frac{d}{ds(t_{\rm f})}(\gamma(s_{\rm ff} - s(t_{\rm f}))) = \gamma \tag{39}$$

From Eqs. (38) and (39), one can conclude that

$$\lambda(t) = \gamma \tag{40}$$

The charge sustaining condition yields $\Delta s_{tf} = 0$, where

$$\Delta s_{\rm rf} \triangleq \int_{t_{\rm r}}^{t_{\rm f}} \dot{s}(\tau) d\tau \tag{41}$$

Finally, the derivatives of the Hamiltonian with respect to the inputs are given as

$$\frac{\partial}{\partial T_e} \dot{m}_f(u(t)) - \lambda \frac{\partial}{\partial T_e} \dot{s}(t) = 0 \tag{42}$$

$$\frac{\partial}{\partial \omega_{e}} \dot{m}_{f}(u(t)) - \lambda \frac{\partial}{\partial \omega_{e}} \dot{s}(t) = 0$$
 (43)

Given the initial values at $t = t_i$ and the driveline's torques and speeds for the entire driving cycle, the optimal solution is obtained by solving Eqs. (34), (38)–(43) for the unknown inputs, $T_{\rm e}(t), \omega_{\rm e}(t), t \in (t_{\rm i}, t_{\rm f})$, the costate, λ , and the battery power, $\hat{P}_{\rm b}(t)$. One can deduce that the solution for any engine power $P_{\rm e}(t) \triangleq T_{\rm e}(t)\omega_{\rm e}(t)$ lies on the most efficient point (subject to the boundary conditions of the engine torque and speed). This fact is confirmed in Ref. [4] by using a stochastic dynamic programming. The union of all these operating points for all engine power, $0 \le P_e \le \max\{P_e\}$, yields a continuous curve on the engine map. An example of the engine map depicting the efficient curve is shown in Fig. 3. We assume that this efficient curve is sufficiently smooth such that it can be estimated offline by an analytical smooth function. Similarly, the instantaneous fuel consumption rate on this curve can be estimated offline by an analytical smooth polynomial function (the curve fit is shown as solid narrow line in Fig. 3). Let $\overline{T}_{e}(\cdot)$ and $\dot{\overline{m}}_{f}(\cdot)$ denote the torque and the instantaneous fuel consumption rate on the efficient curve, respectively. Note that the degree of polynomial can be chosen appropriately such that enough accuracy for curve fitting is achieved. Then, the optimization degrees-of-freedom is reduced to one and the derivative of the Hamiltonian with respect to the input, $u(t) \triangleq \omega_{e}(t)$, is given as

$$\frac{d}{d\omega_{\rm e}} \frac{\dot{m}_{\rm f}(\omega_{\rm e}) - \lambda \frac{d\dot{s}(t)}{dP_{\rm b}} \frac{dP_{\rm b}(t)}{d\omega_{\rm e}} = 0 \tag{44}$$

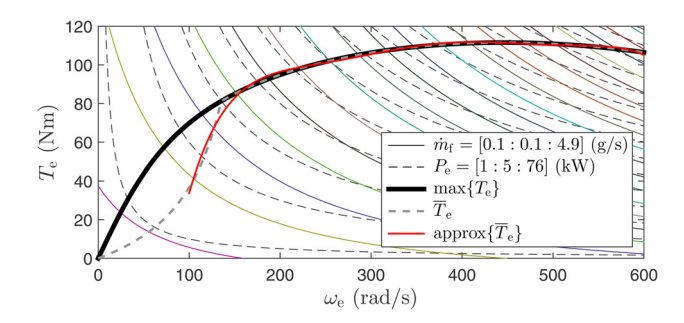


Fig. 3 The fuel consumption map of the internal combustion engine. The polynomial curve fitting in red starts at 100 rad/s since engine normally operates beyond that value.

where

$$\frac{d\dot{s}(t)}{dP_{\rm b}} = \frac{-1}{Q_{\rm b}\sqrt{V_{\rm b}^2 - 4R_{\rm b}P_{\rm b}(t)}}\tag{45}$$

$$\frac{dP_{b}(t)}{d\omega_{e}} = -\mu_{g}^{k_{g}} \frac{d\overline{T}_{e}(\omega_{e})}{d\omega_{e}} \omega_{e}(t) - \mu_{g}^{k_{g}} \overline{T}_{e}(\omega_{e})
- \frac{k_{c} r_{r} \left(\mu_{m}^{k_{m}} - \mu_{g}^{k_{g}}\right)}{r_{s} + r_{r}} \frac{d\overline{T}_{e}(\omega_{e})}{d\omega_{e}} \omega_{d}(t)$$
(46)

Since $\dot{m}_f(\cdot)$ and $\overline{T}_e(\cdot)$ are smooth functions of the engine's speed, they can be estimated by lower order terms in their Taylor expansion as given by (evidenced by the curve fit in red as Fig. 3)

$$\dot{\overline{m}}_{\rm f}(\omega_{\rm e}) \approx \sum_{i=1}^{n_{\rm m}} a_i \omega_{\rm e}^{\rm i}(t) \tag{47}$$

$$\overline{T}_{\rm e}(\omega_{\rm e}) \approx \sum_{i=1}^{n_{\rm t}} b_i \omega_{\rm e}^{\rm i}(t)$$
 (48)

respectively, where $n_{\rm m}, n_{\rm t} \geq 1, \, a_i \in \mathbb{R}, i=1,\ldots,n_{\rm m}$, and $b_i \in \mathbb{R}, i=1,\ldots,n_{\rm t}$. Substituting the above estimation in Eqs (44) and (46) yields the following algebraic equation as

$$\sum_{i=1}^{n_{\rm m}} \left(i a_i \omega_{\rm e}^{i-1}(t) \right) - \lambda \frac{d \dot{s}(t)}{d P_{\rm b}} \frac{d P_{\rm b}(t)}{d \omega_{\rm e}} = 0 \tag{49}$$

and

$$\frac{dP_{b}(t)}{d\omega_{e}} = -\mu_{g}^{k_{g}} \sum_{i=1}^{n_{t}} (i+1)b_{i}\omega_{e}^{i}(t)
-\frac{k_{c}r_{r}\left(\mu_{m}^{k_{m}} - \mu_{g}^{k_{g}}\right)}{r_{s} + r_{r}} \sum_{i=1}^{n_{t}} \left(ib_{i}\omega_{e}^{i-1}(t)\right)\omega_{d}(t)$$
(50)

Given the initial values at $t = t_i$ and the driveline's torques and speeds for the entire driving cycle, the optimal solution is obtained by solving the set of algebraic equations (34), (41), (45), (49), and (50) for the unknown input, $\omega_e(t)$, $t \in (t_i, t_f]$, the costate, λ , and the battery power, $P_b(t)$, subject to the boundary conditions of the powertrain variables. Thus, enabled by the polynomial approximations as Eqs. (47) and (48), the optimal powertrain management can be formulated into a set of algebraic equations.

Remark 4.1. Fuel consumption is a monotonically increasing function of the engine speed on the efficient curve. Therefore, we claim that the estimation of Eq. (47) is fair. Furthermore, an engine efficiency contour map (not shown in the paper) in general

has a smooth gradient from efficient region to low efficient regions and we claim that the optimal curve itself is smooth enough such that the estimations of Eqs. (47)–(48) are feasible.

Remark 4.2. Enabled by approximating the efficient fuel consumption curve as a polynomial of the engine speed, we are able to formulate the PMP constraints into a set of algebraic equations (34), (41), (45), and (47)–(50). This is a novel feature compared with the existing studies of the hybrid vehicles using the PMP [6], where the formulated constraints are a set of differential equations. The algebraic formulation can lead to a computationally efficient real-time optimal solution, enabled by the numerical approach given below.

5 Numerical Solution

The PMP-based approach discussed in Sec. 4 translated the problem to some constraint algebraic equations. Nonetheless, the solution to these equations cannot be obtained analytically nor is the numerical solution trivial. Thus, one may need to advise a practical design for the numerical approach such that its robustness and fast convergence is guaranteed. In order to address this challenge, we give directions on how to solve the constraint algebraic equations specific to the PMP-based formulations given in Sec. 4. The method proposed here is based on the strictness of the hybrid system's constraints. In order to determine the strictness of the constraints, we specify three levels:

The hard or physical constraints: Such constraints give physical relations between system variables and they can be boundary values, algebraic equations, or differential equations. For instance, the utmost operating limits of any of the components in the hybrid system define some physical boundary of the system. Furthermore, any relation between the system's variables such as the power balance equations is considered in this category.

The midlevel or operational constraints: Any limitations for operation of the system set by the designer so as to achieve a better performance, to operate safely, and to increase the life span of the system lie in this category. Such limitations provide a subset of the system's operational region, and thus, do not violate the physical constraints. The limitations on the engine speed, the battery power, and the battery state of the charge are some examples of this type of constraints. Under extreme conditions, these constraints might be violated. For instance, for a continuous very high power on demand at the driveline, the battery can be depleted completely or the output power to the driveline can be limited such that the battery state of charge is preserved. The choice here can depend on the safety measurements of the system.

The soft or optimization constraints: These are specific constraints set by an optimization approach. For instance, the charge sustaining operation of the battery and any algebraic or differential equations obtained through the necessary conditions of the PMP define soft or optimization constraints. These constraints can be disregarded if the physical or the operational constraints are violated. In such cases, the optimal solution might be on the operational boundary.

Next, the numerical approach is designed such that the optimization constraints (soft constraints) appear as corrective terms for the algebraic or differential equations corresponding to the physical (hard) or the operational (midlevel) constraints. Furthermore, the specific optimization variables are adjusted in the outer iterative loop(s), while the system physical variables are adjusted in the inner iterative loop(s). The specific details of the numerical approach for solving Eqs. (34), (41), (45), and (47)–(50) are as follows:

- (1) Acquire the initial values and set $\lambda = 1$ and $P_b = 0$ for the entire driving cycle.
- (2) Calculate Δs_{tf} from Eq. (41).
- (3) Calculate the battery power given by

$$P_{\rm b} = F_{\rm p}(\omega_{\rm e}, \omega_{\rm d}, T_{\rm d}) + K_1 \Delta s_{\rm rf} \tag{51}$$

where $F_p(\cdot,\cdot,\cdot)$ is the right-hand side of Eq. (34) and $K_1 \in \mathbb{R}_+$ is sufficiently small.

- (4) Calculate $\omega_{\rm e}$ by iterating Eq. (34) using the new value of $P_{\rm b}$.
- (5) Calculate other variables of the hybrid system using Eqs. (29)–(32).
- (6) Repeat steps 3–5 for the entire driving cycle.
- (7) Calculate ΔP defined as

$$\Delta P \triangleq \int_{t_{i}}^{t_{f}} \left| \frac{d\dot{m}_{f}(\omega_{e})}{\frac{d\dot{s}(t)}{dP_{b}} \lambda} - dP_{b}(t) \right| \ge 0$$
 (52)

- (8) Calculate Δs_{tf} from Eq. (41).
- (9) If $\Delta P < \Delta P_{\text{min}} > 0$ and $|\Delta s_{\text{rf}}| < \Delta s_{\text{min}} > 0$, stop the iteration for the current driving cycle, else, go to step 10.
- (10) Adjust the costate value as

$$\lambda(k+1) = \lambda(k)(1 - K_2 \Delta s_{\rm rf})(1 - K_3 \Delta P)$$
 (53)

where k is the iteration index, and $K_2, K_3 \in \mathbb{R}_+$ are sufficiently small.

(11) Go to step 3.

Note that the hard/midlevel constraints are checked in steps 3–5, while the optimization constraints appear as corrective terms in steps 3 and 10. Furthermore, note that the outer iteration can be limited to prevent infinite loop in case the optimization problem does not have any solution (for instance, for a very high average power on demand). The analysis on the convergence and robustness of the above approach is conducted through numerical simulation studies given in Sec. 6.

6 Simulation Results

In this section, we provide simulation results in order to evaluate the efficacy of the approaches discussed in this paper. Although the proposed approach is formulated in a generic fashion and can be applied to both off-road and on-road scenarios, we will consider an off-road case as an example in this section. Specifically, we consider a set of identical autonomous off-road hybrid electric vehicles whose parameters are given in Table 1.

In order to evaluate the analytical results provided in Secs. 3 and 4, we consider different case studies. For the first case study, the overall behavior of the distributed optimal cooperative control of the multiagent system of hybrid vehicles is analyzed. For this purpose, we consider the coordinated motion of a set of four autonomous hybrid vehicles and a leader vehicle. The desired formation and communication topology is depicted in Fig. 4 and the leader vehicle's velocity profile is shown in Fig. 5.

We assume $R_{1i} = I_4$, $R_{2i} = I_2$, i = 1,...,p. Accordingly, the LQR control gains are obtained as $K_i = [I_2, 1.7321I_2]$, i = 1,...,p. Finally, we set the initial formation errors and the initial velocities of the vehicles to nonzero values. The results are depicted in Figs. 6–8. Specifically, Fig. 6 shows the phase portrait of the multiagent system, Fig. 7 shows the torque control inputs of each

Table 1 Vehicle system parameters

Parameter	Value	Parameter	Value
m	1350 kg	I	1850 kg/m ²
$I_{ m f}$	2 kg/m^2	$I_{ m r}$	7 kg/m^2
d_{f}	1.5 m	d_{r}	0.9 m
r	0.28 m	f_{t}	0.007
ρ	1.225kg/m^3	$C_{ m d}$	0.3
$A_{ m f}$	2.2 m^2	$k_{\rm c}$	3.9
$r_{\rm s}$	0.030 m	$r_{ m r}$	0.078 m
$\mu_{\rm m},\mu_{\rm g}$	0.9	V_{b}	202 V
Q_{b}	23,400 A.s	R_{b}	0.45Ω

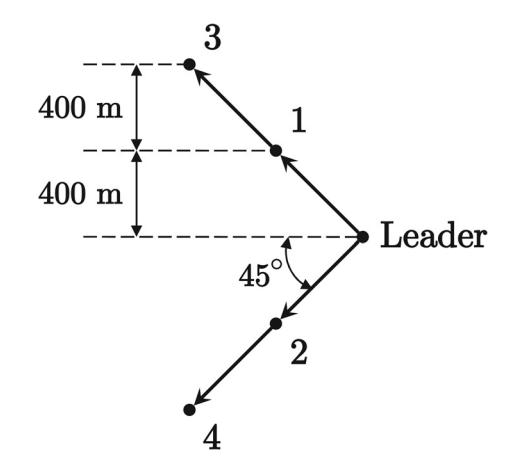


Fig. 4 The communication topology and the desired formation in the multiagent system

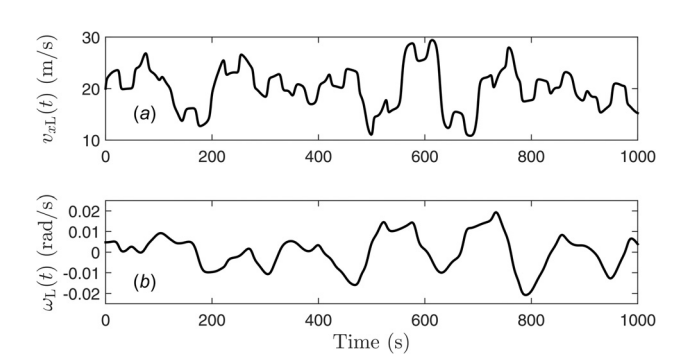


Fig. 5 The velocity profile of the leader vehicle in (a) the longitudinal and (b) the angular directions

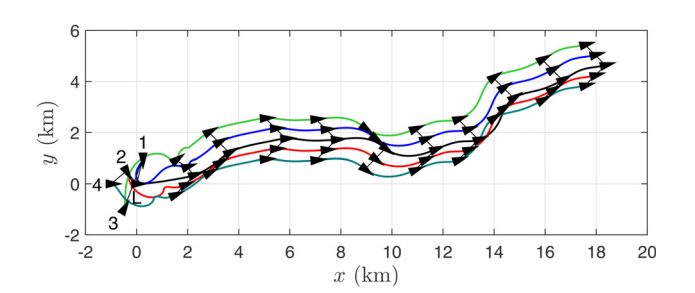


Fig. 6 The phase portrait of the multiagent system

vehicle, and Fig. 8 shows the distributed errors associated with each vehicle.

In order to comply with the limitation of the internal hybrid system of each vehicle, the output control torques are constrained. The limitations depend on the vehicles' speeds and the friction between road and the tires of the vehicles. Thus, at the initial time when the distributed LQR algorithm requires large positive or negative control efforts, saturation happens as shown in Fig. 7. Despite the saturation, the multiagent system performs properly as the distributed formation errors converge to zero (Fig. 8) and the vehicles keep the ">" formation along the way (Fig. 6).

For the next case study, the hybrid powertrain performance is analyzed. We consider the first vehicle in this study as the vehicles are behaving similarly except at the beginning of the cooperation. We consider an internal combustion engine whose fuel consumption map is depicted in Fig. 3. We assume that the operation of the engine is limited to 115 $\leq \omega_e \leq$ 400 rad/s. Furthermore, the battery power is limited to $|P_b| \leq$ 22 kW. For this

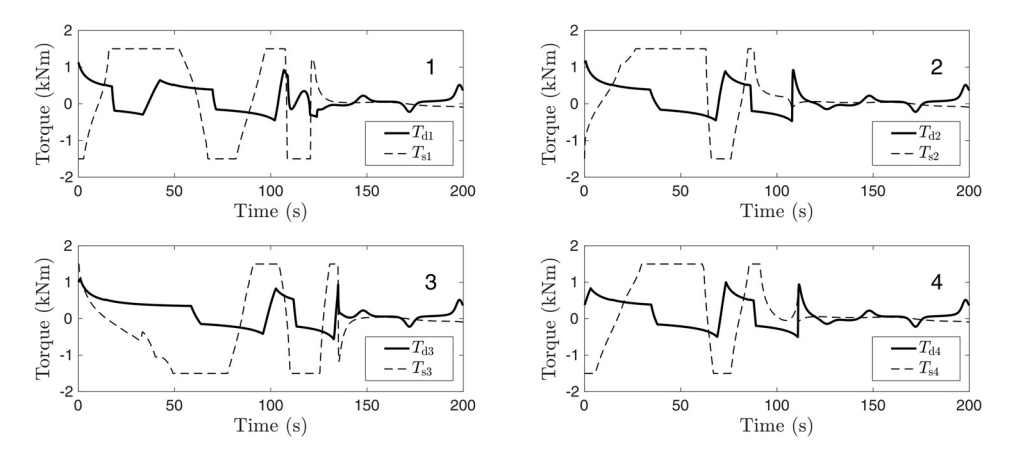


Fig. 7 The time history of the control torques

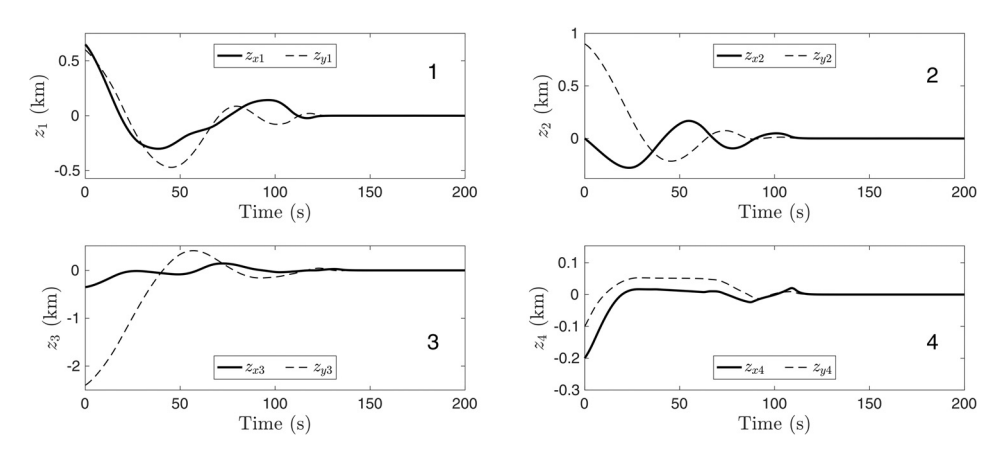


Fig. 8 The time history of the distributed errors

simulation, we set the driving cycle to 1000 s and the initial state of the charge equal to 70%.

The results for the first driving cycle are depicted in Figs. 9–11. Specifically, Fig. 9 shows the time history of input–output power diagrams of the hybrid system, Fig. 10 shows the time history of the state of the charge of the battery, and Fig. 11 shows the time history of the engine's fuel consumption. The hybrid system's response indicate that the battery power is utilized to ensure that engine is dominantly running at the speeds with higher efficiency or otherwise is shut off. The resultant fuel economy is 27.56 km/l.

In order to evaluate the efficiency of the engine, we examine the behavior of the hybrid system in response to different average powers on demand at the driveline. Particularly, we repeat the above simulation for different velocity profiles of the leader vehicle and calculate the overall efficiency of the engine. The results are depicted in Fig. 12 for the average fuel economy and average engine efficiency with respect to the average power on demand. The first diagram indicates that the fuel economy rapidly decreases as the average power on demand increases and it drops to as low as 12 km/l. The purpose of the second diagram is to indicate that the results for different power demands (with wide range of acceleration/deceleration and speeds in highways and urban routes) guarantee highest efficiencies possible. The maximum instantaneous engine efficiency for the engine map shown in Fig. 3 is 16.26 kWs/g, which happens on the efficient curve at engine speeds around 270-305 rad/s. Despite the changes in power demand, the average engine efficiency is almost kept constant for different average power on demands and it is very close to the maximum instantaneous engine efficiency. Furthermore, the engine operation is more sensitive to the temporal details of the

powers on demand at the lower average powers on demand. The resultant fluctuations vanish as the average power on demand increases

In the next case studies, we evaluate the performance of the numerical approach for solving the PMP-based formulation of the optimization in the hybrid system. First, we examine the effects of the driving cycle on the stability of the method. We set the sampling time-step in optimization to 0.1 s and repeat the simulation for an extended time interval. Figure 13 depicts the maximum simulation time and the maximum number of iterations versus driving cycle.

The processor used in this study is an Intel[®] Quad CoreTM i5 CPU with 3.33 GHz computational frequency and the main solver code is written in C programming language. The result indicates that for small driving cycles, the convergence is slower (higher iterations) while for high driving cycles, the convergence rate is almost constant. The convergence is at the highest rate (lowest iterations) for the driving cycle equal to 1000 s. Furthermore, the computation time is slowly decreasing for driving cycles up to 1000 s, where it is minimum. For higher values of the driving cycles, the computation time increases rapidly, which is almost proportional to the values of the driving cycles.

Next, we examine the effect of the optimization sampling timestep. Figure 14 provides the computational statistical results for different sampling time steps and driving cycles. The results indicate that the sampling time steps and convergence rate (which is inversely proportional to the number of iterations) are not correlated. Thus, the computation time is reversely proportional to the sampling time-step. The above results give a hint that a rough yet acceptable solutions can be obtained for high values of the

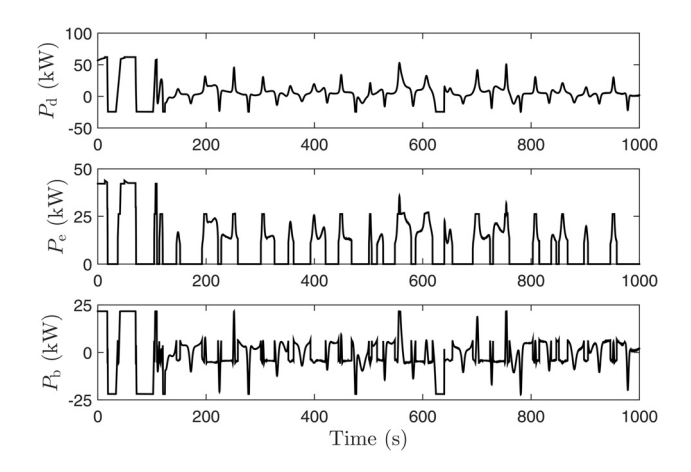


Fig. 9 The time history of the input-output powers to/from the hybrid systems through the driveline, the engine, and the battery, respectively

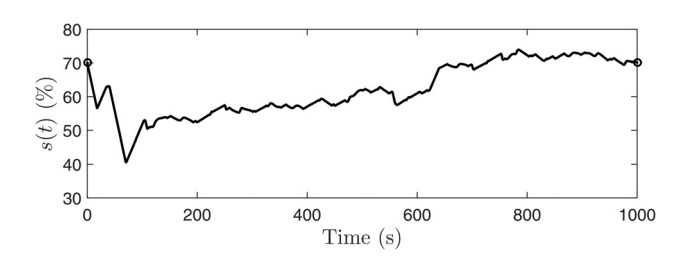


Fig. 10 The time history of the state of the charge of the battery

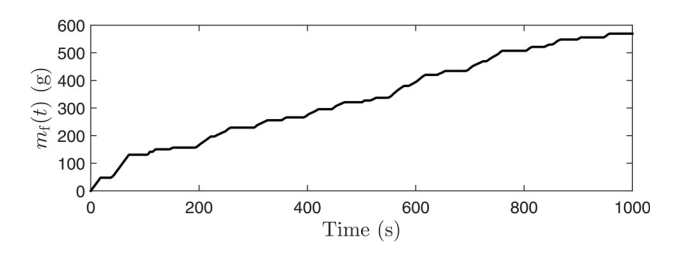


Fig. 11 The time history of the fuel consumption by the engine

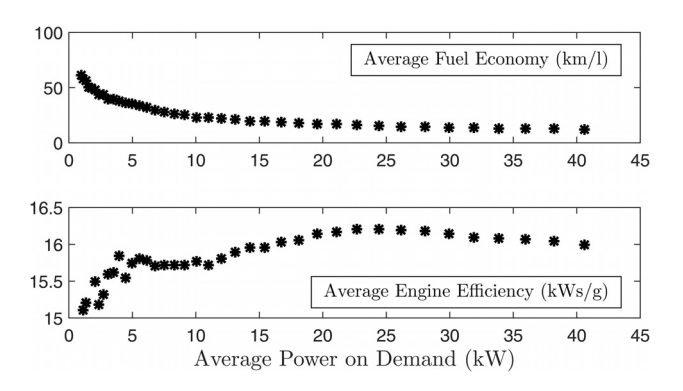


Fig. 12 The efficiency metrics of the engine

sampling time-step (for instance, 1 s), and then, they can be further adjusted with lower sampling time steps. Therefore, the computational cost and time is decreased greatly. The above studies offer that the methodology proposed in this paper is computationally efficient for real-time implementation.

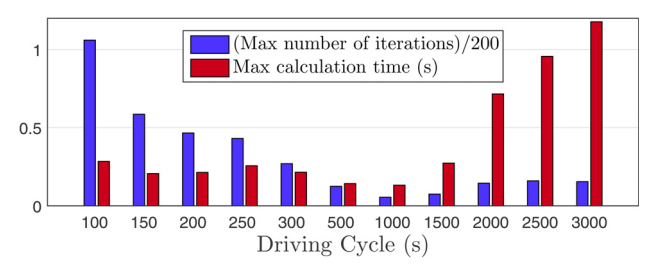


Fig. 13 The effect of the driving cycle on the performance of the numerical approach

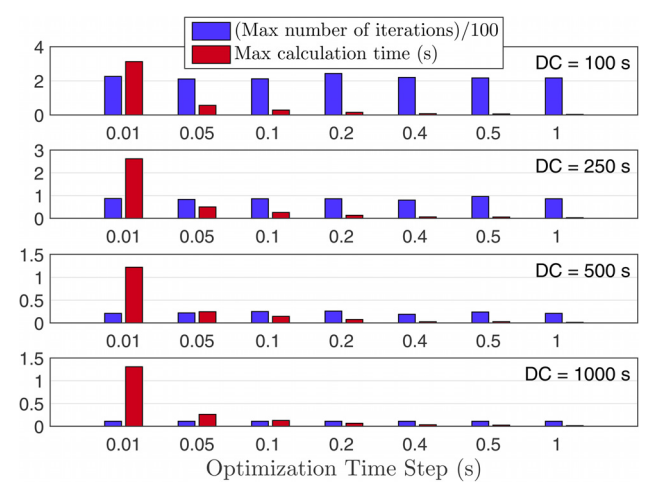


Fig. 14 The effect of the optimization sampling time-step on the performance of the numerical approach for different driving cycles

7 Conclusion

In this paper, we considered the powertrain energy management in multiple autonomous and connected hybrid electric vehicles. The optimization process was given in two successive steps. In the first step, the distributed locally optimal solution for the nonlinear multiagent system was derived. The formulation was given first for the Euler-Lagrangian agents' dynamics in an affine structure and then extended to our specific nonlinear vehicular dynamics through coordinate transformation. The future vehicle driveline power demand can then be determined and predicted based on the multi-agent cooperative controller. In the second step, based on the predicted power demand, the hybrid powertrain energy management was optimized by using Pontryagin's minimum principle. Specifically, we gave a fully analytical formulation of the optimization problem subject to the hybrid system's constraints and assuming that the future information of the powers on demand (torques and speeds at the driveline) are available. The formulation resulted in some constrained algebraic equations, enabled by approximating the optimal instantaneous fuel consumption rate as a polynomial of the engine speed. We provided the directions on a numerical iterative approach to solve these equations. Through statistical analysis, we confirmed its stability and robustness for different driving cycles and sampling time steps in optimization. Furthermore, we provided simulation case studies so as to evaluate the efficacy and the robustness of the proposed optimal approaches.

Funding Data

 National Science Foundation (Grant No. 1826410; Funder ID: 10.13039/501100008982).

Appendix: Model of an Autonomous Vehicle

Consider the rear wheel-driven vehicle whose free body diagram is shown in Fig. 1. The global position and orientation coordinates of the vehicle are determined by variables X, Y, and θ , respectively. The kinematics of the vehicle are given by

$$\dot{X}(t) = v_x(t)\cos\theta(t) - v_y(t)\sin\theta(t) \tag{A1}$$

$$\dot{Y}(t) = v_x(t)\sin\theta(t) + v_y(t)\cos\theta(t)$$
 (A2)

$$\dot{\theta}(t) = \omega(t) \tag{A3}$$

where v_x and v_y are the projections of the velocity of the mass center C onto the body fixed frame, and ω is the angular velocity of the vehicle around the Z axis, the axis orthogonal to the X-Y plane. Furthermore, the Newtonian equations of motion are given by

$$m\dot{v}_x(t) - m\omega(t)v_v(t) = f_{1r}(t) - f_{1f}(t) - f_{D}$$
 (A4)

$$m\dot{v}_{y}(t) + m\omega(t)v_{x}(t) = f_{2r}(t) + f_{2f}(t)$$
 (A5)

$$I\dot{\omega}(t) = d_{\rm f}f_{\rm 2f}(t) - d_{\rm r}f_{\rm 2r}(t) + T_{\rm f}(t) + T_{\rm r}(t)$$
 (A6)

where $f_{1\rm r}$ and $f_{2\rm r}$ are the equivalent longitudinal and lateral friction forces acting on the rear wheels' midaxle, respectively. $f_{1\rm f}$ and $f_{2\rm f}$ are the equivalent longitudinal and lateral friction forces acting on the front wheels' midaxle, respectively, $T_{\rm r}$ and $T_{\rm f}$ are the equivalent torques due to longitudinal friction forces on the rear and the front wheels, respectively, and $f_{\rm D}$ is the drag force. We define the steering torque as

$$T_{\rm s}(t) \triangleq d_{\rm f} f_{\rm 2f}(t) + T_{\rm f}(t) + T_{\rm r}(t)$$
 (A7)

We assume that the equivalent torques $T_{\rm r}$ and $T_{\rm f}$ are negligible so as to avoid dynamical redundancy. Thus, the steering torque is estimated as

$$T_{\rm s}(t) \approx d_{\rm f}f_{\rm 2f}(t)$$
 (A8)

Furthermore, we assume that the resultant dynamics obey the non-holonomic constraint restricting the motion of the wheels to pure rolling with no slip in the lateral directions. This assumption is true for an ideal Ackermann steering mechanism. Thus, one can write

$$v_{\rm v}(t) = \dot{\theta}(t)d_{\rm r}, \quad t > 0$$
 (A9)

Since Eq. (A9) is valid at all times, its time derivative yields

$$\dot{v}_{\nu}(t) = \ddot{\theta}(t)d_{\rm r}, \quad t > 0 \tag{A10}$$

Substituting Eqs. (A10) and (A8) in Eq. (A5) gives

$$f_{2r}(t) = md_r\dot{\omega}(t) + m\omega(t)v_x(t) - \frac{1}{d_r}T_s(t)$$
 (A11)

The rear longitudinal friction force, f_{1r} , is obtained by considering the dynamics of the active rear wheels

$$f_{1r}(t) = \frac{1}{r} T_{\rm d}(t) - \frac{I_{\rm r}}{r^2} \dot{v}_x(t)$$
 (A12)

where $T_{\rm d}$ is the vehicle's driving torque acting on the rear wheels' axle. Since, the vehicle's motion obeys the nonholonomic constraint of pure rolling and no slip motion, then we can substitute it by a single wheel placed at the front midaxle. The orientation and the velocity of this virtual wheel are equal to those of the front midaxle point. Therefore, the kinematics of this wheel are derived as

$$\omega(t) = \frac{1}{d_{\rm f} + d_{\rm r}} v_{\rm f}(t) \sin \alpha(t)$$
 (A13)

$$v_x(t) = v_f(t)\cos\alpha(t)$$
 (A14)

where ν_f is the velocity of the virtual wheel and $\alpha \in (-(\pi/2), (\pi/2))$ is the orientation of the virtual wheel in the body fixed frame. The time derivative of Eqs. (A13) and (A14) yields

$$\frac{\dot{v}_{\rm f}(t)}{\cos\alpha(t)} = \dot{v}_{x}(t) + \frac{(d_{\rm f} + d_{\rm r})^2 \omega(t)}{v_{x}(t)} \dot{\omega}(t) \tag{A15}$$

Furthermore, the dynamics of the virtual wheel is given as

$$f_{\rm lf}(t)\cos\alpha(t) - f_{\rm 2f}(t)\sin\alpha(t) = \frac{I_{\rm f}}{r^2}\dot{v}_{\rm f}(t)$$
 (A16)

Substituting Eqs. (A8) and (A13)–(A15) in Eq. (A16) yields

$$f_{1f}(t) = \frac{(d_{f} + d_{r})\omega(t)}{d_{f}v_{x}(t)} T_{s}(t) + \frac{I_{f}}{r^{2}} \dot{v}_{x}(t) + \frac{(d_{f} + d_{r})^{2}\omega(t)}{r^{2}v_{x}(t)} \dot{\omega}(t)$$
(A17)

Finally, the drag force is given by

$$f_{\rm D}(t) = \frac{1}{2} \rho C_{\rm d} A_{\rm f} v_x^2(t)$$
 (A18)

Substituting the relations for the friction forces and the drag force in the equations of motion (A4) and (A6) gives

$$M(\eta)\dot{\eta}(t) = F(\eta) + G(\eta)T(t) \tag{A19}$$

where $\eta \triangleq [v_x, \omega]^T$ is the velocity vector, $T \triangleq [T_d, T_s]^T$ is the vector of driving and steering torques,

$$M(\eta) \triangleq \begin{bmatrix} \tilde{m} & \frac{I_{\rm f}(d_{\rm f} + d_{\rm r})^2 \omega(t)}{r^2 v_x(t)} \\ 0 & \tilde{I} \end{bmatrix}$$
(A20)

$$F(\eta) \triangleq \begin{bmatrix} md_{\rm r}\omega^2(t) - \frac{1}{2}\rho C_{\rm d}A_{\rm f}v_x^2(t) - f_{\rm t}mg \\ -md_{\rm r}\omega(t)v_x(t) \end{bmatrix}$$
(A21)

$$G(\eta) \triangleq \begin{bmatrix} \frac{1}{r} & -\frac{(d_{\rm f} + d_{\rm r})\omega(t)}{d_{\rm f}v_x(t)} \\ 0 & \frac{d_{\rm f} + d_{\rm r}}{d_{\rm f}} \end{bmatrix}$$
(A22)

 $\tilde{m} \triangleq m + ((I_{\rm f} + I_{\rm r})/r^2)$, $\tilde{I} \triangleq I + md_{\rm r}^2$, and $f_{\rm t}$ is the friction coefficient. Note that the penalty term f_t mg added to the above derivation so as to consider practical surface reaction for friction force when wheels slip.

References

- [1] Kim, H., and Kum, D., 2016, "Comprehensive Design Methodology of Inputand Output-Split Hybrid Electric Vehicles: In Search of Optimal Configuration," IEEE/ASME Trans. Mechatronics, 21(6), pp. 2912–2923.
- [2] Kim, S. J., Kim, K. S., and Kum, D., 2016, "Feasibility Assessment and Design Optimization of a Clutchless Multimode Parallel Hybrid Electric Powertrain," IEEE/ASME Trans. Mechatronics, 21(2), pp. 774–786.
- [3] Panday, A., and Bansal, H. O., 2014, "A Review of Optimal Energy Management Strategies for Hybrid Electric Vehicle," Int. J. Veh. Technol., 2014, p. 160510.
- [4] Liu, J., and Peng, H., 2008, "Modeling and Control of a Power-Split Hybrid Vehicle." IEEE Trans. Control Syst. Technol., 16(6), pp. 1242–1251.
- Vehicle," IEEE Trans. Control Syst. Technol., 16(6), pp. 1242–1251.
 [5] Chasse, A., and Sciarretta, A., 2011, "Supervisory Control of Hybrid Powertrains: An Experimental Benchmark of Offline Optimization and Online Energy Management," Control Eng. Pract., 19(11), pp. 1253–1265.

- [6] Kim, N., Cha, S., and Peng, H., 2011, "Optimal Control of Hybrid Electric Vehicles Based on Pontryagin's Minimum Principle," IEEE Trans. Control Syst. Technol., 19(5), pp. 1279–1287.
- [7] Kim, N., Cha, S., and Peng, H., 2012, "Optimal Equivalent Fuel Consumption for Hybrid Electric Vehicles," IEEE Trans. Control Syst. Technol., 20(3), pp. 817–825.
- [8] Kim, N., Rousseau, A., and Lee, D., 2011, "A Jump Condition of PMP-Based Control for PHEVs," J. Power Sources, 196(23), pp. 10380–10386.
 [9] Mohd-Zulkefli, M. A., Zheng, J., Sun, Z., and Liu, H. X., 2014, "Hybrid Power-
- [9] Mohd-Zulkefli, M. A., Zheng, J., Sun, Z., and Liu, H. X., 2014, "Hybrid Power-train Optimization With Trajectory Prediction Based on Inter-Vehicle-Communication and Vehicle-Infrastructure-Integration," Transp. Res. Part C, 45, pp. 41–63.
- [10] Stockar, S., Marano, V., Rizzoni, G., and Guzzella, L., 2010, "Optimal Control for Plug-In Hybrid Electric Vehicle Applications," American Control Conference (ACC), Baltimore, MD, June 30–July 2, pp. 5024–5030.
- [11] Haddad, W. M., and Chellaboina, V., 2008, Nonlinear Dynamical Systems and Control. A Lyapunov-Based Approach, Princeton University Press, Princeton, NJ.
- [12] Movric, K. H., and Lewis, F. L., 2014, "Cooperative Optimal Control for Multi-Agent Systems on Directed Graph Topologies," IEEE Trans. Autom. Control, 59(3), pp. 769–774.
- [13] Zhang, H., Feng, T., Yang, G. H., and Liang, H., 2015, "Distributed Cooperative Optimal Control for Multiagent Systems on Directed Graphs: An Inverse Optimal Approach," IEEE Trans. Cybern., 45(7), pp. 1315–1326.

- [14] Zhang, H., Lewis, F. L., and Qu, Z., 2012, "Lyapunov, Adaptive, and Optimal Design Techniques for Cooperative Systems on Directed Communication Graphs," IEEE Trans. Ind. Electron., 59(7), pp. 3026–3041.
- [15] Nedic, A., Ozdaglar, A., and Parrilo, P. A., 2010, "Constrained Consensus and Optimization in Multi-Agent Networks," IEEE Trans. Autom. Control, 55(4), pp. 922–938.
- [16] Zhang, H., Zhang, J., Yang, G. H., and Luo, Y., 2015, "Leader-Based Optimal Coordination Control for the Consensus Problem of Multi-Agent Differential Games Via Fuzzy Adaptive Dynamic Programming," IEEE Trans. Fuzzy Syst., 23(1), pp. 152–163.
- [17] Mesbahi, M., and Egerstedt, M., 2010, Graph Theoretic Methods in Multiagent Networks, Princeton University Press, Princeton, NJ.
- [18] Chalanga, A., Kamal, S., Fridman, L. M., Bandyopadhyay, B., and Moreno, J. A., 2016, "Implementation of Super-Twisting Control: Super-Twisting and Higher Order Sliding-Mode Observer-Based Approaches," IEEE Trans. Ind. Electron., 63(6), pp. 3677–3685.
- [19] Levant, A., and Livne, M., 2018, "Globally Convergent Differentiators With Variable Gains," Int. J. Control, 91(9), pp. 1–15.
- [20] Ghasemi, M., Nersesov, S. G., and Clayton, G., 2014, "Finite-Time Tracking Using Sliding Mode Control," J. Franklin Inst., 351(5), pp. 2966–2990.
- [21] Adachi, S., and Hagihara, H., 2012, "The Renewed 4-Cylinder Engine Series for Toyota Hybrid System," 33rd International Vienna Motor Symposium, Vienna, Austria, Apr., pp. 1–24.